PCCP

PAPER

View Article Online
View Journal | View Issue

Cite this: *Phys. Chem. Chem. Phys.*, 2023, **25**, 5656

In silico capture and activation of methane with light atom molecules†

Stefan Mebs *[a] and Jens Beckmann [b]

Methane (CH_4) can be captured *in silico* with a light atom molecule containing only C, H, Si, O, and B atoms, respectively. A tripodal *peri*-substituted ligand system was employed, namely, [(5-Ph_2B-xan-4-)$_3$-Si]H (**1**, xan = xanthene), which after hydride abstraction (**1$^+$**) carries four Lewis acidic sites within the cationic cage structure. In a previous study, this system was shown to be able to capture noble gas atoms He–Kr (Mebs & Beckmann 2022). In the corresponding methane complex, **1$^+$CH$_4$**, a polarized $Si^+\cdots CH_4$ contact of 2.289 Å as well as series of $(H_3)CH\cdots O/C_{Ph}$ hydrogen bonds enforce spatial CH_4 fixation (the molecule obeys C_3-symmetry) and slight activation. A trigonal-pyramidal $Si{-}CH^{eq}{}_3{-}H^{ax}$ local geometry is thereby approached with $H^{ax}{-}C{-}H^{eq}$ angles decreased to 103.7°. All attempts to replace the Lews acidic $-BPh_2$ fragments in **1** with basic $-PR_2$ (R = Ph, *t*Bu) fragments indeed increased intra-molecular hydrogen bonding between host molecule and CH_4, and thus caused stronger activation of the latter, however ultimately resulted in the formation of energetically favorable quenched structures with short P–Si contacts, making CH_4 binding hard to achieve. The electronic situation of two hypothetic methane complexes, **1$^+$CH$_4$** and [(5-*t*Bu_2P-xan-4-)$_3$$SiCH_4$]$^+$ (**2$^+$CH$_4$**), was determined by a set of calculated real-space bonding indicators (RSBIs) including the Atoms-In-Molecules (AIM), non-covalent interactions index (NCI), and electron localizability indicator (ELI-D) methods, highlighting crucial differences in the level of activation. The proposed ligand systems serve as blueprints for a more general structural design with adjustable trigonal ligand systems in which central atom, spacer fragment, and functional *peri*-partner can be varied to facilitate different chemical tasks.

Received 13th December 2022,
Accepted 25th January 2023

DOI: 10.1039/d2cp05821a

rsc.li/pccp

Introduction

Methane is the main component in natural gas, a key molecule in chemical synthesis and the second most important greenhouse gas, thus of global relevance for modern society. Moreover, it is a highly inert molecule, which resists trapping and its use as source for value added products requires energy consumptive conversion into syngas (CO + H_2) at high temperatures.[1] Of particular industrial relevance is the separation of CH_4 from CO_2 and N_2. Besides cryogenic distillation, different adsorbent-based techniques are applied.[2] In a large-scale computational study, the potential of liquid solvents or zeolite structures to capture methane was addressed, but with limited success.[3] Experimental studies employed metal–organic frameworks (MOFs) to selectively bind CO_2 over CH_4 (enriching the latter)[4] or adsorb CH_4 under high pressure or recently even under ambient conditions.[5,6] Methane indeed is trapped in enormous quantities as methane hydrate (also methane clathrate, methane ice, fire ice,...) within water crystal structures in the shallow maritime geosphere and permafrost, and as such may have a massive effect on the world climate when the average temperature rises further.[7] To date, however, light-atom organic molecular guest–host complexes with CH_4 are yet unknown, to the best of our knowledge, and no X-ray diffraction study of such a complex was published.[8,9] Indirect proof of CH_4-complex formation with noble transition metals such as Rh were given by different kinds of spectroscopy, such as NMR.[10] A metal-free activation of methane by a borenium complex was recently published, but the procedure requires 60 bar of CH_4 and 110 °C to give reasonable yields.[11]

We describe here a computational study on the first two molecular transition-metal free methane complexes, one of which potentially could be formed under ambient conditions. In our conceptual DFT screening approach we previously found that a tripodal *peri*-system ligand design with a central silyl cation as central linker, and suitable combinations of spacer fragments, such as acenaphthene or xanthene, with Lewis acidic and/or basic *peri*-, such as $-BPh_2$ or $-PPh_2$ groups, which serve as secondary functional groups, allows to successfully address important chemical tasks such as N_2 or CO_2 activation

[a] *Institut für Experimentalphysik, Freie Universität Berlin, Arnimallee 14, 14195, Berlin, Germany. E-mail: stefan.mebs@fu-berlin.de*
[b] *Institut für Anorganische Chemie und Kristallographie, Universität Bremen, Leobener Straße 7, 28359, Bremen, Germany*

† Electronic supplementary information (ESI) available. See DOI: https://doi.org/10.1039/d2cp05821a

and capture of noble gases.[12–15] In the course of fixing and activation of methane we exploit the C_3-symmetry of particular tailor-made ligand systems, which guarantees an ideal embedment of the tetrahedral guest molecule within the active site (or void) of the surrounding host molecule. The first ligand system, [(5-Ph_2B-xan-4-)$_3$Si]H (**1**, xan = xanthene), contains four Lewis acidic sites and itself is actually also capable to energy efficiently fix noble gases.[13] The second ligand system, [(5-^{t}Bu_2P-xan-4-)$_3$Si]H (**2**), combines the Lewis acidic silyl cation in the center with three Lewis basic –PPh_2 groups in the side-arms, which results in considerably stronger fixation and activation of CH_4, actually facilitating its subsequent deprotonation, but unfortunately suffers from premature quenching. In our screening approach, we could exclude several other spacer molecules, such as naphthalene (d_{peri} = 2.5 Å), acenaphtene (d_{peri} = 2.7 Å), biphenylene (d_{peri} = 3.9 Å), and dibenzofuran (d_{peri} = 5.4 Å) to provide suitable hosts for methane. Xanthene apparently has a proper *peri*-distance (d_{peri} = 4.9 Å), offers a hydrogen bond donor (the O-atoms), and is flexible to accommodate for structural changes associated with CH_4-uptake. Moreover, xanthene is a common organic molecule, derivatives of which are widely used in chemical industry, *e.g.* for dyes. A potential synthesis route of compound **1** is given in Scheme S1 (ESI†).

DFT calculations

Structural optimizations were conducted for all compounds by density functional theory (DFT) at the B3PW91/6-31 + G*[16,17] level of theory using Gaussian16[18] at the curta super-computer system of the Freie Universität Berlin. London dispersion was modelled using Grimme's GD3BJ parameters.[19] The COSMO solvation model was applied to mimic the dichloromethane environment.[20] Normal mode (or frequency) analysis proved the relaxed geometries of all but one relevant states to be local minima on the potential energy hypersurface and provided ΔG values. A weak negative frequency of -21.6 cm^{-1}, which is a torsion motion on one *tert*-butyl group, remained for $\mathbf{2^+CH_3}$ (see below), despite efforts to reoptimize the structure. Potential energy scans (PES) with fixed Si···C(H_4) distances have been conducted for both CH_4-adducts ($\mathbf{1^+CH_4}$, $\mathbf{2^+CH_4}$) in order to understand the "entry behavior" of CH_4 into the hosts voids and to quantify it energetically, however, due to complex potential energy profiles (*e.g.* rotation motion of CH_4 against the host molecules), the optimizations mostly didn't fully converge even after long calculation times, so they were stopped when energetic changes didn't exceed 1 kJ mol^{-1} over several steps. The transition state ($\mathbf{2^+TS}$) relevant for the CH_4 deprotonation step was calculated using the QST3-algorythm of Gaussian16. It shows a strong negative band of -714.4 cm^{-1}, which corresponds to the migration of the abstracted proton from C- to P-atom, *i.e.* $H_3C\cdots H\cdots PR_3$. As a consequence of the complexity of the structural analysis, some energetic trends are discussed by means of ΔE (*e.g.* structural isomerism), others in ΔG (*e.g.* reaction steps). The electronic structure of the CH_4-adducts, the transition state towards methane deprotonation, and of the reaction product ($\mathbf{2^+CH_3}$) was extracted from the calculated electron and electron pair densities employing the Atoms-In-Molecules – AIM[21–23] (topological analysis of the electron density with AIM2000[24]), Electron-Localizability-Indicator – ELI-D[25] (bonding and lone-pair basin analysis with DGRID-5-1;[26] grid step size: 0.05 a.u.), and non-covalent interactions index – NCI[27] (intra-molecular contact patches with NCIplot;[28] grid step size: 0.07 a.u.) toolkits. Analyses of the reduced density gradient, $s(\mathbf{r}) = [1/2(3\pi^2)^{1/3}]|\nabla\rho|/\rho^{4/3}$, according to the NCI method is used to visualize non-covalent bonding aspects. An estimation of different non-covalent contact types according to steric/repulsive ($\lambda_2 > 0$, red-colored), van der Waals-like ($\lambda_2 \approx 0$, green-colored), and attractive ($\lambda_2 < 0$, blue-colored) is facilitated by mapping the ED times the sign of the second eigenvalue of the Hessian ($\mathrm{sign}(\lambda_2)\rho$) on the iso-surfaces of $s(\mathbf{r})$. For ELI-D figures, additional grids of 0.15 a.u. step size were computed. Structures are displayed with GaussView, bond paths are displayed with AIM2000, NCI and ELI-D figures are displayed with MolIso.[29]

Results and discussion

In order to capture and activate methane with a light-atom host molecule of the here proposed type a number of criteria have to be fulfilled, which we stepwise address (the molecular design should of course be rational, *i.e.* the ligand system should be principally accessible by synthetic chemistry): 1. the pre-active neutral state as well as the charged/activated state of the ligand system are likely prone to conformational isomerism and the void-forming conformer should be either the lowest in energy or at least energetically accessible; 2. Hydride abstraction and formation of the methane complex should be exergonic or at least only slightly endergonic to provide a stable compound, which is potentially accessible by structural determination techniques like X-ray diffraction; 3. While methane enters the host, the latter needs to change its conformation temporarily to give access to the void, which shouldn't be too energy consumptive, *i.e.* a low CH_4 entry-barrier is demanded.

Compound **1**: we investigate first the capability of ligand system [(5-Ph_2B-xan-4-)$_3$Si]H (**1**, xan = xanthene) to form a suitable activated host molecule after hydride abstraction ($\mathbf{1^+}$) and to give access to a stable CH_4-complex ($\mathbf{1^+CH_4}$), see Fig. 1, 2, Fig. S1 and S2 (ESI†) as well as Tables S1 and S2 (ESI†). Its criteria represent as follows:

1. The neutral starting compound **1** potentially exists in three different conformational isomers, two of which are void-forming after hydride abstraction ("*endo*"- or "*exo*"-variant of **1**; both providing $\mathbf{1^+_{active}}$, see below), one of which is not ("dead"-variant). The *exo*-conformation ($\mathbf{1}_{exo}$, Fig. S1a, ESI†) would principally be preferred as starting material, as the Si–H section is located at the outer-sphere of the ligand system and is thus easy accessible by hydride abstraction agents, however, this conformation is 103 kJ mol^{-1} higher in energy (ΔE) compared to its *endo*-counterpart ($\mathbf{1}_{endo}$, Fig. S1c, ESI†). Advantageously, the unfavored dead-conformation ($\mathbf{1}_{dead}$, Fig. S1b, ESI†) is also 35 kJ mol^{-1} higher in energy compared to "*endo*", making the

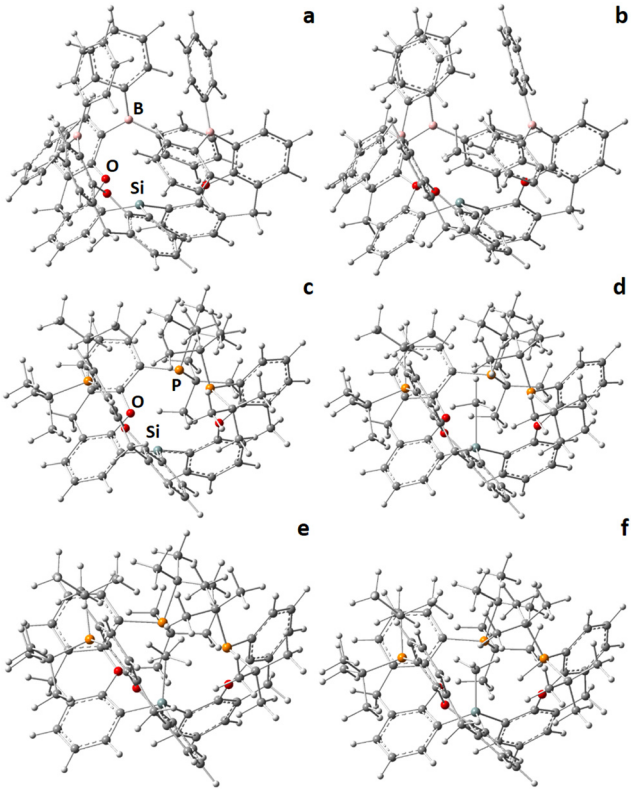

Fig. 1 Structures of $\mathbf{1}^+$ (a), $\mathbf{1}^+\mathbf{CH_4}$ (b), $\mathbf{2}^+\mathbf{C_3}$ (c), $\mathbf{2}^+\mathbf{CH_4}$ (d), $\mathbf{2}^+\mathbf{TS}$ (e), $\mathbf{2}^+\mathbf{CH_3}$ (f).

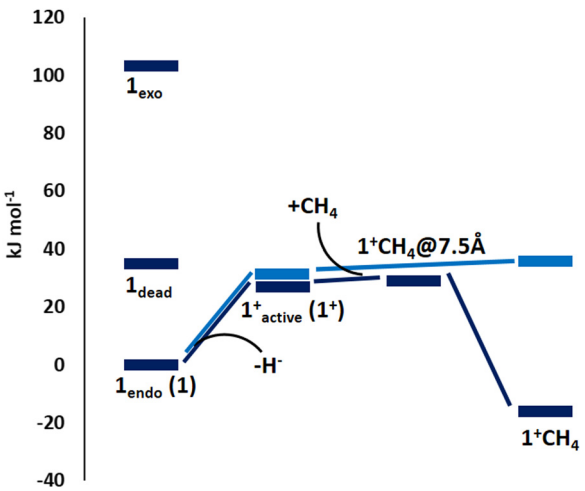

Fig. 2 Relative energies (ΔE, dark blue) of structural isomers (*e.g. exo*-, dead-, and *endo*-variants of the neutral starting state **1**, or methane complex of $\mathbf{1}^+$ with the CH_4-fragment at different Si···CH_4 distances, which serve as rough estimate for transition states for CH_4 complex formation) and relative enthalpies (ΔG, light blue) of different electronic states. The energy of the *endo*-conformer of **1** was set to zero. ΔG of $\mathbf{1}^+\mathbf{CH_4}$ is corrected for BSSE and 1-atm-to-1-M conversion.

latter the likely main product in ligand synthesis. Accordingly, $\mathbf{1}_{endo}$ is labeled as **1** in the following. The charged compound, $\mathbf{1}^+$, principally also exists in two conformational isomers, one of which is void-forming ($\mathbf{1}^+_{active}$, Fig. S1d, ESI†), one of which is not ($\mathbf{1}^+_{dead}$, Fig. S1e, ESI,† 17.1 kJ mol^{-1} lower in energy than $\mathbf{1}^+_{active}$), but since hydride abstraction from $\mathbf{1}_{endo}$ causes formation of $\mathbf{1}^+_{active}$, the three Si–C_{xan} bonds now exhibit partial double-bond character, and rotation along this bond would be accompanied with a significant rotational energy barrier, it can be excluded at this stage. Accordingly, $\mathbf{1}^+_{active}$ is labeled as $\mathbf{1}^+$ in the following.

2. The reaction enthalpy (ΔG) of the hydride abstraction step to form the active state $\mathbf{1}^+$ from **1** is calculated to be slightly endergonic ($\Delta G_{(\mathbf{1}\rightarrow\mathbf{1}^+)}$ = 31.5 kJ mol^{-1}, Fig. 1a and 2), which is assumed to be feasible under common reaction conditions (*e.g.* slightly elaborated temperatures). The reaction enthalpy of the subsequent CH_4-complex formation step to form $\mathbf{1}^+\mathbf{CH_4}$ (Fig. 1b and 2) from $\mathbf{1}^+$ is almost enthalpy-neutral ($\Delta G_{(\mathbf{1}^+\rightarrow\mathbf{1}^+\mathbf{CH_4})}$ = 4.2 kJ mol^{-1}). This value already includes correction for basis-set superposition error (BSSE = 4.0 kJ mol^{-1}) and conversion from 1 atm to 1 M condition (7.9 kJ mol^{-1}).

3. By keeping the Si···C_{CH4} distance fixed to 5, 7.5, 10, and 12.5 Å (restrained optimizations, Fig. S2, ESI†), the energy barrier (ΔE) for gaseous CH_4 to enter $\mathbf{1}^+$ was estimated to be only about 2 kJ mol^{-1} (at d(Si···C_{CH4}) = 7.5 Å), so energetic costs induced by bending of the host molecule to form $\mathbf{1}^+\mathbf{CH_4}$ are considered negligible. When CH_4 further approaches the Si center, 57.2 kJ mol^{-1} are released, which in return means the exit barrier of CH_4 in $\mathbf{1}^+\mathbf{CH_4}$ is equally large. In other words, once formed, $\mathbf{1}^+\mathbf{CH_4}$ should form a stable complex.

In summary, controllable rotational isomerism of the starting material, medium to small positive reaction enthalpies of hydride abstraction and CH_4 complex formation, and a negligible CH_4 entry barrier into the void of the host, but a considerable CH_4 exit barrier, render formation of $\mathbf{1}^+\mathbf{CH_4}$ feasible with moderate synthetic efforts. $\mathbf{1}^+\mathbf{CH_4}$ would then be the first stable methane complex employing a light-atom molecule. In order to account for the level of theory (particular the lack of polarization functions on the H-atoms), single-point calculations were performed at the B3PW91/6-311 + G(2df,p) level using the structural coordinates optimized at the lower B3PW91/6-31 + G* level, see Table S1 (ESI†). Since the geometries were not optimized at the higher level, the results may be considered as semi-quantitative, but it should be noted that the overall trends found at the lower level are fully conserved, and that the two crucial steps of hydride abstraction and CH_4-complex formation become more favorable at the higher level by 5–13 kJ mol^{-1}, which gives further confidence into our results.

Compound **2**: a considerably more complex and less controllable situation, however, is unfortunately obtained for the [(5-*t*Bu_2P-xan-4-)$_3$Si]H (**2**) analogue, see Fig. 1, and Fig. S3–S6 as well as Tables S1 and S2 (ESI†). Its criteria represent as follows:

1. As in **1**, three rotational isomers are relevant for the neutral starting state of **2**, which show equal relative energies ($\mathbf{2}_{endo}$ is 91 kJ mol^{-1} lower in energy than $\mathbf{2}_{exo}$ and 49 kJ mol^{-1} lower in energy than $\mathbf{2}_{dead}$, Fig. S3a–c, ESI†). Accordingly, $\mathbf{2}_{endo}$ is labeled as **2** in the following. But in contrast to $\mathbf{1}^+$, which forms only one relevant structural isomer, $\mathbf{2}^+$ diverges in at least

three different isomers, one obeying C_3-symmetry ($\mathbf{2^+C_3}$, void-forming, Fig. S3d, ESI†) with three Si···P distances of 4.608 Å, an asymmetric one being 6.1 kJ mol^{-1} lower in energy ($\mathbf{2^+C_1}$, potentially void-forming, Fig. S3e, ESI†) with Si···P distances of 4.530, 4.614, and 4.727 Å, as well as a quenched state being 46.9 kJ mol^{-1} lower in energy ($\mathbf{2^+_{quench}}$, not void-forming, Fig. S3f, ESI†) exhibiting a very short Si–P distance of 2.470 Å, likely preventing CH_4 uptake. $\mathbf{2^+_{dead}}$ (Fig. S3g, ESI†) was also calculated, and is even 75.5 kJ mol^{-1} lower in energy than $\mathbf{2^+C_3}$, but considered inaccessible, thus negligible.

2. The reaction enthalpy (ΔG) of the hydride abstraction step to form the active state $\mathbf{2^+C_3}$ from **2** is calculated to be almost enthalpy-neutral ($\Delta G_{(2\rightarrow 2+C3)}$ = 7.0 kJ mol^{-1}, Fig. 1c), even better values are of course expected if $\mathbf{2^+C_1}$ or $\mathbf{2^+_{quench}}$ are considered as product (not shown). The reaction enthalpy of the subsequent CH_4-complex formation step to form $\mathbf{2^+CH_4}$ (Fig. 1d) from $\mathbf{2^+C_3}$ is also almost enthalpy-neutral ($\Delta G_{(2+C3\rightarrow 2+CH4)}$ = 7.2 kJ mol^{-1}); taking $\mathbf{2^+_{quench}}$ as reference, a much less favorable value is obtained ($\Delta G_{(2+q\rightarrow 2+CH4)}$ = 35.5 kJ mol^{-1}). These values again include correction for basis-set superposition error (BSSE = 5.6 kJ mol^{-1}) and conversion from 1 atm to 1 M condition (7.9 kJ mol^{-1}).

3. By keeping the Si···C_{CH4} distance fixed to 2.5, 3.0, 3.5, 4.0, 4.5, and 5.0 Å (restrained optimizations, Fig. S4, ESI†), the energy barrier (ΔE) for gaseous CH_4 to enter $\mathbf{2^+C_3}$ was estimated to be about 90 kJ mol^{-1} (at d(Si···C_{CH4}) = 4.5 Å, Fig. S4f, ESI†), so energetic costs induced by bending of the host molecule to form $\mathbf{2^+CH_4}$ are significant, as $\mathbf{2^+}$ preferably would form a short Si–P bond ($\mathbf{2^+_{quench}}$) and CH_4 would remain at the outer side of the ligand system ($\mathbf{2^+CH_{4(exo)}}$, Fig. S4h, ESI†). Once $\mathbf{2^+CH_4}$ would be formed, however, it would experience a large exit barrier (72 kJ mol^{-1}), and since CH_4 is considerably activated in $\mathbf{2^+CH_4}$, it would preferably be deprotonated than leave, see below, as well as Fig. S6 (ESI†) for more details of the energy scheme.

In summary, unfavorable structural isomerism of the activated material, a significantly positive reaction enthalpy of CH_4 complex formation starting from the quenched active state, as well as a considerable CH_4 entry barrier into the void of the host, render formation of $\mathbf{2^+CH_4}$ feasible only with elaborated synthetic efforts, such as purging of the neutral ligand system **1** with pressurized methane *via* hydride abstraction, if at all. It remains to be seen if variation of the spacer fragment or the *peri*-partner can solve this issue, and DFT-work is ongoing in this direction.

In $\mathbf{1^+CH_4}$, the methane molecule is only slightly activated. To the contrast, it is significantly more strongly bound and notably more activated in $\mathbf{2^+CH_4}$ and requires only 17 kJ mol^{-1} to be deprotonated by the host molecule; the transfer of the proton to the non-bonding electron pair of an adjacent P atom thereby releases considerable 182 kJ mol^{-1}. As the bound CH_4 would need a higher amount of energy to leave the void as gaseous CH_4 again (exit barrier), being trapped once by $\mathbf{2^+}$ is likely an irreversible process for methane.

Real-space bonding indicator analysis: despite the fact that formation of $\mathbf{2^+CH_4}$ apparently is not a trivial task, we were interested in the bonding situation of both methane complexes, which were thus analyzed in detail computationally using a suitable set of real-space bonding indicators (RSBI), providing insight into strengths and nature of primary and secondary atom–atom interactions within these complex molecular systems (Fig. 3 and 4 and Table 1).

A zoom-in of the AIM bond topology of $\mathbf{1^+CH_4}$ and $\mathbf{2^+CH_4}$ (see ESI† for full molecule representations) unravels the formation of a Si–CH_4 bond critical point (bcp) in both cases (highlighted by a blue arrow in Fig. 3a and 4a), indicating a direct chemical interaction between the silyl cationic center and the CH_4 molecule. The Si–CH_4 bond distance is remarkable (2.289 Å) in $\mathbf{1^+CH_4}$ but astonishing (2.081 Å) in $\mathbf{2^+CH_4}$, which is accompanied by structural deformation of CH_4 towards a Si–CH_3–H trigonal bipyramid, particularly in $\mathbf{2^+CH_4}$. Both complexes thereby retained the C_3-symmetry of their parent compounds. With electron density (ED, $\rho(\mathbf{r})_{bcp}$) values of 0.27 or 0.41 e Å^{-3} the Si–CH_4 contacts are substantially stronger than hydrogen bonds, and the fact that both the kinetic energy density over ED ratio ($G/\rho(\mathbf{r})_{bcp}$) as well as the total energy density over ED ratio ($H/\rho(\mathbf{r})_{bcp}$) are considerably positive or negative, respectively, highlights the relevance of both covalent and non-covalent bonding aspects to these interactions. This is corroborated by inspection of NCI contact patches and ELI-D basins. On the one hand, NCI exhibits a blue-colored disc- or ring-shaped Si–CH_4 basin (highlighted by a yellow arrow in Fig. 3b and 4b) signifying attractive non-covalent bonding aspects. On the other hand, a Si–C ELI-D bonding basin is preformed in $\mathbf{1^+CH_4}$, but already topologically separated and fully formed in

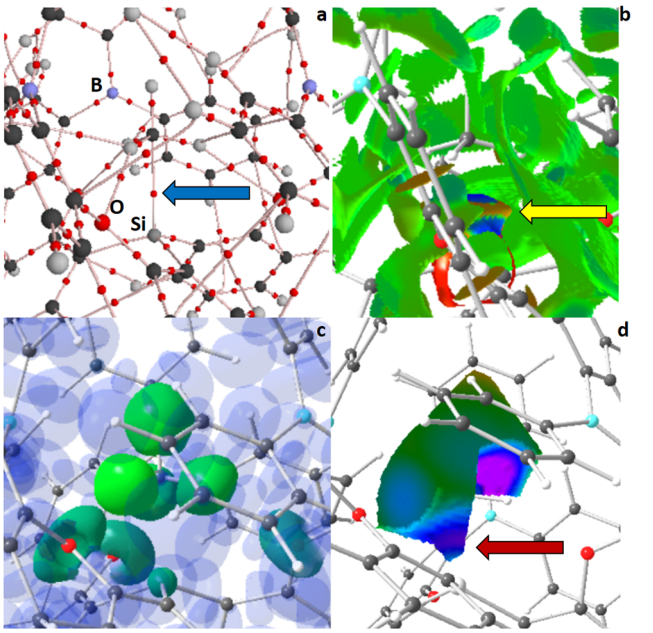

Fig. 3 RSBI analysis of $\mathbf{1^+CH_4}$ (a) AIM bond paths motif, (b) NCI isosurface at $s(\mathbf{r})$ = 0.5, (c) ELI-D localization domain representation at an isovalue of 1.4, (d) ELI-D distribution mapped on two H_{CH4} ELI-D basins (equatorial and axial). Color code atoms: hydrogen – light gray, carbon – medium gray, oxygen – medium red, phosphor – dark or pale red, boron – light blue.

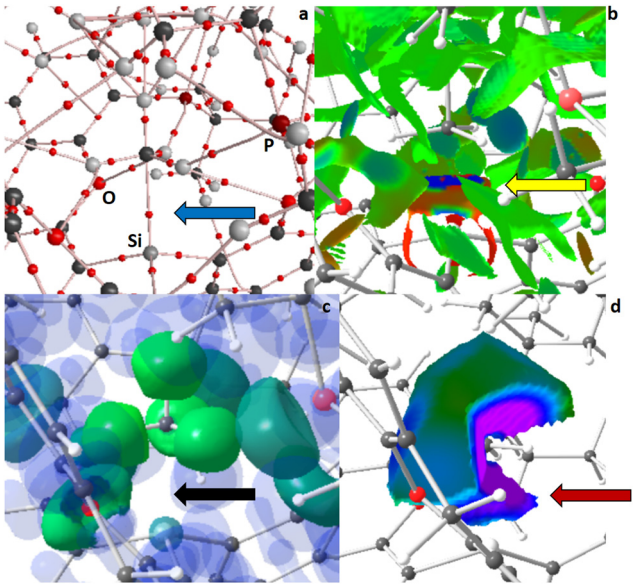

Fig. 4 RSBI analysis of $\mathbf{2^+CH_4}$ (a) AIM bond paths motif, (b) NCI iso-surface at $s(\mathbf{r})$ = 0.5, (c) ELI-D localization domain representation at an iso-value of 1.4, (d) ELI-D distribution mapped on two H_{CH4} ELI-D basins (equatorial and axial). Color code atoms: hydrogen – light gray, carbon – medium gray, oxygen – medium red, phosphor – dark or pale red.

Table 1 Geometric and electronic parameters of the methane complexes

Model	d_{C-H1} [Å]	d_{C-H2} [Å]	d_{C-H3} [Å]	d_{C-H4} [Å]	H1–C–H4 [°]	H2–C–H4 [°]	H3–C–H4 [°]
$\mathbf{1^+CH_4}$	1.099			1.099	103.7		
$\mathbf{2^+CH_4}$	1.116			1.096	97.8		
$\mathbf{2^+TS}$	1.091	1.125	1.254	1.095	114.2	92.5	89.3
$\mathbf{2^+CH_3}$	1.091	1.091	2.687	1.090	108.0	107.2	

Model	d_{Si-C} [Å]	d_1/d	$\rho(\mathbf{r})_{bcp}$ [eÅ^{-3}]	$\nabla^2\rho(\mathbf{r})_{bcp}$ [eÅ^{-5}]	ε	$G/\rho(\mathbf{r})_{bcp}$ [a.u.]	$H/\rho(\mathbf{r})_{bcp}$ [a.u.]
$\mathbf{1^+CH_4}$	2.289	0.78	0.27	0.9	0.00	0.56	−0.34
$\mathbf{2^+CH_4}$	2.081	0.74	0.41	2.5	0.00	0.86	−0.43
$\mathbf{2^+TS}$	2.010	0.73	0.55	3.2	0.15	0.93	−0.52
$\mathbf{2^+CH_3}$	1.878	0.72	0.80	6.1	0.01	1.13	−0.60

Model	Q^{AIM}_{lig} [e]	Q^{AIM}_{CHn} [e]	Q^{AIM}_{C} [e]	N_{ELI} [e]	V_{ELI} [Å^3]	γ_{ELI}	RJI [%]
$\mathbf{1^+CH_4}$	0.95	0.06	−0.43				
$\mathbf{2^+CH_4}$	1.02	−0.02	−0.72	0.38	1.0	1.36	72.0
$\mathbf{2^+TS}$	1.11	−0.11	−0.87	1.07	2.9	1.64	81.4
$\mathbf{2^+CH_3}$	1.69	−0.67	−0.80	2.00	5.9	2.02	85.2

H1–3 are equatorial, H4 is axial; $\rho(\mathbf{r})_{bcp}$: ED at the bcp, $\nabla^2\rho(\mathbf{r})_{bcp}$: laplacian, ε: bond ellipticity d_1: distance atom(1)-bcp, $G/\rho(\mathbf{r})_{bcp}$, $H/\rho(\mathbf{r})_{bcp}$: kinetic and total energy density over $\rho(\mathbf{r})_{bcp}$ ratios, Q^{AIM}: AIM fragmental and atomic charges, N_{ELI}, V_{ELI}: electron populations and volumes the ELI-D basin, γ_{ELI}: ELI-D value at the attractor position, RJI: Raub–Jansen Index; Q^{AIM}_C = −0.12 e for gaseous CH_4.

$\mathbf{2^+CH_4}$ (highlighted by a red arrow in Fig. 3d and 4d), pointing towards non-negligible covalent bonding aspects of these polarized-covalent bonds. However, the Si–C ELI-D basin is small (V_{ELI} = 1.0 Å^3), little populated (N_{ELI} = 0.38 e), and not fully "localized" (γ_{ELI} = 1.36), so it's not (yet) visible at a common iso-surface of γ = 1.4 (highlighted by a black arrow in Fig. 4c). The NCI further shows small blueish-colored disc-shaped CH···O/P basins as well as extended greenish-colored flat areas, and AIM shows numerous CH···O/P/C/H bcps, altogether representing a plethora of secondary intramolecular interactions, such as hydrogen bonds, H···H contacts, and van-der-Waals interactions, which stabilize the guest within the host. Similar bonding conditions were observed in noble-gas (Ng) complexes of **1**, in which $\mathbf{1^+He}$ and $\mathbf{1^+Ne}$ showed only a Si–Ng NCI basin but no corresponding ELI-D bonding basin, indicating the dominance of non-covalent bonding aspects, whereas a Si–Ng ELI-D bonding basin was additionally formed in $\mathbf{1^+Ar}$ and $\mathbf{1^+Kr}$, indicating rising covalent bond contributions.[13] CH_4-complex formation is also accompanied by strongly increased internal polarization within the CH_4-fragment, as well as minor charge transfer between ligand system and CH_4, which is reflected in AIM atomic and fragmental charges (Table 1).

The activation of methane in $\mathbf{2^+CH_4}$ is pronounced enough to make the transition state ($\mathbf{2^+TS}$) towards deprotonation only 16.7 kJ mol^{-1} higher in energy, as mentioned above. A nearby lone-pair of a P atom serves as acceptor for that proton. In the TS, the CH_4-fragment is bent/flattened and one C–H bond is extended to 1.254 Å (Fig. 5 and Table 1). A new CH···P AIM bcp is formed (highlighted by a light blue arrow in Fig. 5a), the NCI exhibits a blue-colored ring-shaped CH···P basin (orange arrow in Fig. 5b), and the ELI-D shows strongly increased localizability on the H-basin (a so-called protonated valence basin) in direction of the P atom (purple arrow in Fig. 5d). In the process of deprotonation, the Si–C ELI-D basin becomes larger (V_{ELI} = 2.9 Å^3), more populated (N_{ELI} = 1.07 e), and more localized (γ_{ELI} = 1.64), making it visible at γ = 1.4. In accordance, the bond becomes shorter and the ED at the Si–CH_4 bcp rises up to

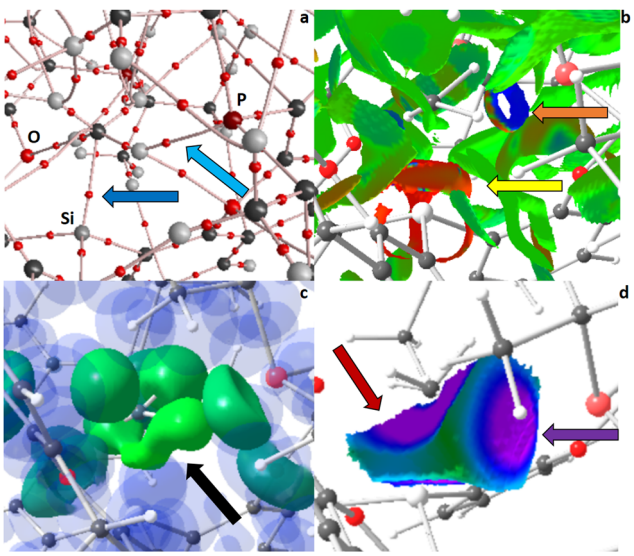

Fig. 5 RSBI analysis of $\mathbf{2^+TS}$ (a) AIM bond paths motif, (b) NCI iso-surface at $s(\mathbf{r})$ = 0.5, (c) ELI-D localization domain representation at an iso-value of 1.4, (d) ELI-D distribution mapped on the newly formed Si–C_{CH4} ELI-D basin and the H basin, which is going to be transferred to the P atom. Color code atoms: hydrogen – light gray, carbon – medium gray, oxygen – medium red, phosphor – dark or pale red.

0.55 e Å^{-1}. Notably, the Si–C ELI-D basin and two equatorial H basins are topologically connected in **2$^+$TS** (black arrow in Fig. 5c), which they weren't in **2$^+$CH$_4$**. After the deprotonation is completed, the former lone-pair basin of the P atom (a non-bonding valence basin) has become a protonated valence-basin, which is topologically fully separated from the new R_3Si^+–CH_3 part of the molecule (Fig. S7, ESI† and Table 1). The Si–C ELI-D basin becomes even larger (V_{ELI} = 5.9 Å^3), more populated (N_{ELI} = 2.00 e), and more localized (γ_{ELI} = 2.02), now resembling a "conventional" Si–C bonding basin, with even shorter bond distance and increased ED at the bcp ($\rho(\mathbf{r})_{bcp}$ = 0.80 e Å^{-1}). The Raub–Jansen-Index (RJI) combines AIM and ELI-D and is an indicator of bond-polarity; the range spans from 50–60% for homo-polar bonds, from roughly 60–90% for polarized-covalent interactions, from 90–98% for dative and ionic bonds, to about 100% for purely van-der-Waals-like contacts. The Si–CH_n (n = 4 or 3) lies in the typical range for polarized-covalent contacts, supporting the statements above, and the polarization is increasing in the series **2$^+$CH$_4$** → **2$^+$TS** → **2$^+$CH$_3$**. The charge-transfer from ligand system to CH_n-fragment and the internal polarization of the CH_n-fragment itself are also increasing along that series (Table 1).

Conclusion

Our computational study shows that it is possible to capture and potentially also activate methane exploiting the tripodal design and symmetry of a light-atom molecule such as [(5-Ph_2B-xan-4-)$_3$Si]H (**1**). In **1**, which formally contains four Lewis acidic functional sites, the electron density of the B–C_{Ph} bonds serve as weak hydrogen bonding acceptor instead; attempts to further increase intramolecular hydrogen bond strengths by replacing the –BPh_2 by –P*t*Bu_2 groups, however, makes synthesis of the corresponding methane complex hard to achieve due to premature quenching of the activated state. Work is ongoing to find a balanced molecular design, which captures and activates CH_4 in order to make it accessible for subsequent chemical transformations.

Conflicts of interest

The authors declare no conflicts of interest.

Acknowledgements

The DFG is acknowledged for funding.

References

1 T. V. Choudhary and V. R. Choudhary, *Angew. Chem., Int. Ed.*, 2008, **47**, 1828–1847.
2 A. Alonso, J. Moral-Vico, A. A. Markeb, M. Busquets-Fite, D. Komilis, V. Puntes, A. Sanchez and X. Font, *Sci. Total Environ.*, 2017, **595**, 51–62.
3 J. Kim, A. Maiti, L. C. Lin, J. K. Stolaroff, B. Smit and R. D. Aines, *Nat. Commun.*, 2013, 4.
4 Y. C. Lin, C. L. Kong, Q. J. Zhang and L. Chen, *Adv. Energy Mater.*, 2017, 7.
5 Z. Niu, X. L. Cui, T. Pham, P. C. Lan, H. B. Xing, K. A. Forrest, L. Wojtas, B. Space and S. Q. Ma, *Angew. Chem., Int. Ed.*, 2019, **58**, 10138–10141.
6 R. B. Lin, L. B. Li, A. Alsalme and B. L. Chen, *Small Struct.*, 2020, **1**(3), 2000022.
7 K. A. Kvenvolden, *Chem. Geol.*, 1988, **71**, 41–51.
8 M. D. Walter, P. S. White, C. K. Schauer and M. Brookhart, *New J. Chem.*, 2011, **35**, 2884–2893.
9 V. D. Makhaev, *Usp. Khim.*, 2003, **72**, 287–310.
10 W. H. Bernskoetter, C. K. Schauer, K. I. Goldberg and M. Brookhart, *Science*, 2009, **326**, 553–556.
11 Y. Z. Liu, W. S. Dong, Z. H. Li and H. D. Wang, *Chem*, 2021, **7**, 1843–1851.
12 S. Mebs and J. Beckmann, *Phys. Chem. Chem. Phys.*, 2022, **24**, 20953–20967.
13 S. Mebs and J. Beckmann, *Phys. Chem. Chem. Phys.*, 2022, **24**, 20968–20979.
14 S. Mebs, *Chem. Phys. Chem.*, 2022, e202200621.
15 S. Mebs and J. Beckmann, *Chem. Phys. Chem.*, submitted.
16 A. D. Becke, *J. Chem. Phys.*, 1993, **98**, 1372–1377.
17 J. P. Perdew, J. A. Chevary, S. H. Vosko, K. A. Jackson, M. R. Pederson, D. J. Singh and C. Fiolhais, *Phys. Rev. B: Condens. Matter Mater. Phys.*, 1992, **46**, 6671–6687.
18 M. J. T. Frisch, G. W. Schlegel, H. B. Scuseria, G. E. Robb, M. A. Cheeseman, J. R. Scalmani, G. Barone, V. Petersson, G. A. Nakatsuji, H. Li, X. Caricato, M. Marenich, A. V. Bloino, J. Janesko, B. G. Gomperts, R. Mennucci, B. Hratchian, H. P. Ortiz, J. V. Izmaylov, A. F. Sonnenberg, J. L. Williams-Young, D. Ding, F. Lipparini, F. Egidi, F. Goings, J. Peng, B. Petrone, A. Henderson, T. Ranasinghe, D. Zakrzewski, V. G. Gao, J. Rega, N. Zheng, G. Liang, W. Hada, M. Ehara, M. Toyota, K. Fukuda, R. Hasegawa, J. Ishida, M. Nakajima, T. Honda, Y. Kitao, O. Nakai, H. Vreven, T. Throssell, K. Montgomery, J. A. Peralta Jr., J. E. Ogliaro, F. Bearpark, M. J. Heyd, J. J. Brothers, E. N. Kudin, K. N. Staroverov, V. N. Keith, T. A. Kobayashi, R. Normand, J. Raghavachari, K. Rendell, A. P. Burant, J. C. Iyengar, S. S. Tomasi, J. Cossi, M. Millam, J. M. Klene, M. Adamo, C. Cammi, R. Ochterski, J. W. Martin, R. L. Morokuma, K. Farkas, O. Foresman, J. B. Foresman and D. J. Fox, *Gaussian 09, Revision C.01*, Gaussian, Inc., Wallingford CT, 2016.
19 S. Grimme, *J. Comput. Chem.*, 2006, **27**, 1787–1799.
20 S. Miertus, E. Scrocco and J. Tomasi, *Chem. Phys.*, 1981, **55**, 117–129.
21 R. F. W. Bader, *Bull. Am. Phys. Soc.*, 1977, **22**, 305–306.
22 R. F. W. Bader and T. T. Nguyendang, *Adv. Quantum Chem.*, 1981, **14**, 63–124.
23 R. F. W. Bader, *Acc. Chem. Res.*, 1985, **18**, 9–15.
24 F. Biegler-Konig, J. Schonbohm and D. Bayles, *J. Comput. Chem.*, 2001, **22**, 545–559.

25 M. Kohout, *Int. J. Quantum Chem.*, 2004, **97**, 651–658.
26 *DGRID-5.1*, ed. M. Kohout, Radebeul, 2015.
27 E. R. Johnson, S. Keinan, P. Mori-Sanchez, J. Contreras-Garcia, A. J. Cohen and W. T. Yang, *J. Am. Chem. Soc.*, 2010, **132**, 6498–6506.
28 J. Contreras-Garcia, E. R. Johnson, S. Keinan, R. Chaudret, J. P. Piquemal, D. N. Beratan and W. T. Yang, *J. Chem. Theory Comput.*, 2011, **7**, 625–632.
29 C. B. Hübschle and P. Luger, *J. Appl. Crystallogr.*, 2006, **39**, 901–904.

